Analyst

PAPER

View Article Online
View Journal

Cite this: DOI: 10.1039/c4an02159b

Tandem differential mobility spectrometry with ion dissociation in air at ambient pressure and temperature

M. R. Menlyadiev, A. Tarassov, A. M. Kielnecker and G. A. Eiceman*

Received 23rd November 2014,
Accepted 13th March 2015

DOI: 10.1039/c4an02159b

www.rsc.org/analyst

Proton-bound dimers were dissociated to protonated monomers in air at ambient pressure and temperature using electric fields of ultrahigh Field Asymmetric Ion Mobility Spectrometry (ultraFAIMS) with the onset of dissociation for ethyl acetate as 96 Td and for dimethyl methyl phosphonate as 170 Td. Ions then were measured by differential mobility spectrometry (DMS). Fragment ions were formed with propyl acetate at electric fields of 90 Td or greater. The dissociation in ultraFAIMS of ions, with compensation fields near zero, to form smaller ions with new compensation fields, provided a method to improve peak capacity in DMS without gas modifiers. These findings also lay the foundation for a triple stage DMS with a centre stage for ion dissociation or fragmentation.

Introduction

Differential mobility spectrometry (DMS) is a relatively recent embodiment for ion mobility measurements where gas phase ions are characterized using field-dependent mobilities near or at ambient pressure in purified nitrogen, air, or other gas mixtures.[1–4] Various configurations have been developed for use as ion filters with mass spectrometers,[5–8] as hand-held detectors for chemical warfare agents,[9] as benchtop trace detectors of explosives,[9] and as a portable gas chromatograph-differential mobility spectrometer for air quality monitoring on the International Space Station.[10]

Response to vapour samples in DMS originates when an analyte enters the ion source and is ionized, often through chemical ionization reactions at atmospheric pressure (APCI). Such reactions occur in positive polarity through displacement mechanisms where a substance, M, displaces water from $H^+(H_2O)_n$, forming $MH^+(H_2O)_{n-1}$. In negative polarity, similar reactions occur to form $MO_2^-(H_2O)_{n-1}$. Some selectivity in analytical response is already introduced into a mobility measurement from ionization properties, where a substance forms either a stable positive ion or a negative ion but commonly not both. In addition, the reactant ion $H^+(H_2O)_n$ can be altered with a reagent gas (R) as found in chemical ionization mass spectrometry forming $H^+(R)_n$ with increases in the selectivity of response. An advantage of APCI reactions is that analyte mass is concentrated in a single or perhaps two ion peaks, improving limits of detection and lessening the demand on resolving power of the mobility analysers.

In mobility spectra of DMS, ion peaks appear at characteristic compensation voltages (CV), or compensation fields (CF), which are used to restore the ion passage through the drift tube from off-axis displacement associated with field dependence of ion mobility. This dependence is found in the expression for ion mobility in DMS, $K(E/N)$, where E/N is the field strength normalized to gas number density in eqn (1):

$$K(E/N) = K_o(1 + \alpha(E/N)) \quad (1)$$

with an alpha function, $\alpha(E/N)$, describing the relationship between $K(E/N)$ and E/N for an ion at a given temperature in a gas of a particular composition.[11] The standard unit for E/N is Townsend (Td) and 1 Td = 10^{-17} V cm^{-2}. This dependence arises through a combination of behaviours which can also be observed in low field mobility measurements.[12] One process involves the formation and dissociation of ion clusters that form between ions and polarizable gases or gas atmospheres containing polar constituents. These ion–dipole associations are favoured at low temperature (and low E/N) and are pronounced with ion mass below 100 Da.[13] In DMS, these are seen as positive alpha dependences where ΔK, the difference in mobilities at strong and weak electric fields, increases with E/N and ion peaks are displaced proportionally from 0 V on the CV scale. As the ion mass increases, the effect of small neutral adducts on the alpha function is lessened, ΔK is smaller, and the ion peak approaches 0 V on the CV scale. A second behaviour for ions in electric fields is decreased mobility when field strengths are increased. This can be observed in

Department of Chemistry and Biochemistry, New Mexico State University, 1175 North Horseshoe Drive, Las Cruces, NM 88003-8001, USA. E-mail: geiceman@nmsu.edu, marlen@nmsu.edu

any gas, both clustering and non-clustering, and usually at high E/N values. This produces a negative alpha function and negative ΔK where the ion peak is displaced from 0 CV, opposite in polarity to ions with the positive ΔK values.[14] Such a behaviour becomes noticeable for ion masses of 300 Da or greater. Ions between 100 and 300 Da may exhibit a positive alpha function in early stages of E/N, which turns negative when the ion is declustered at large E/N, leaving only the increased resistance to motion by collisions.

A practical implication of the described ion behaviour in DMS is that the analytical space is limited for ions with a mass of 100–300 Da, where peaks can be clustered on the compensation field axis within a few peak widths around 0 Td.[17] This condition can be improved through modification of the alpha functions by the addition of small neutral molecules into the supporting gas atmosphere including water, methylene chloride and alcohols.[15–17] In recent years, this concept has been developed with significantly improved analytical performance in mobility-mass spectrometry[18,19] and has been extended to the measurement of larger ions.[20] Despite being successful, more than one modifier is needed for a broad range of ion identities.[21,22] A complementary facet of ion behaviour and technology of DMS is the capability to vary and sweep the voltage (or E/N) on the separation waveform to provide a measure of the alpha function in so-called dispersion plots.[23] Such dispersion plots provide a measure of the fundamental ion behaviour and can guide the selection of parameters for the best resolving power. The determination of dispersion plots is relatively time-consuming, and a recent embodiment of DMS with tandem stages each with characteristic pairs of compensation and separation voltages (CV and SV) was used to exploit patterns of ion dependence in dispersion plots with response times of 100 ms.[24]

Discussions on ion motion in DMS usually presume stability of ions during a measurement, although some substances form ions which can decompose in air at ambient pressure when heated thermally or electrically. A first thorough description of the instability of ions in ion mobility spectrometry (IMS) drift tubes at ambient pressure was given for ions of butyl acetates above 100 °C.[25] Later, ion transformations were documented and measured for the dissociation of proton-bound dimers of amines[26] and substitution and charge exchange reactions of explosives.[27] These studies demonstrated that ion dissociations and fragmentations can be controlled by the effective temperature of ions, T_{eff}, and reactions occur on timescales of mobility measurements at ambient pressure. In addition to heat from the gas atmosphere, ion energy can be affected by electric fields and ions can be dissociated or fragmented by electric fields which can reach 30 000 V cm^{-1} for 300 ns or more in DMS. Examples include the dissociation of dimer ions of dimethyl methylphosphonate (DMMP)[28] and fragmentation of esters[29] and methyl salicylate.[30] Early findings suggested that the transfer of energy to an ion leading to dissociation or fragmentation is dependent on ion mass, and fields of 30 000 V cm^{-1} or ~150 Td were insufficient for large ions at low temperatures.

Technology suitable for generating electric fields of 250 Td, or ~60 000 V cm^{-1} in air, sufficient to dissociate or fragment comparatively large ions, is available in ultrahigh Field Asymmetric Ion Mobility Spectrometry (ultraFAIMS) devices which have been commercialized recently as ion pre-filters for mass spectrometers.[31] An attractive feature of such strong fields is the possibility of dissociating ions at or near room temperature in hand-held portable DMS instruments, increasing the analytical space by reagent free ion transformation to a small ion with increased alpha function. The goal of this work is to develop and explore the analytical capabilities of a tandem mobility instrument, herein an ultraFAIMS/DMS combination, in place of a single stage DMS and to lay the foundation for a triple stage DMS which includes ion selection, ion fragmentation, and characterization of product ions for mobility. The specific objective of the current study is to explore the dissociation of gas ions near room temperature by high fields of ultraFAIMS with subsequent characterization of these ions by DMS.

Experimental

Instrumentation

The tandem mobility spectrometer (Fig. 1) was composed of a first stage ultraFAIMS device (adapted from the UltraFAIMSK-DK1 Developer Kit from Owlstone Nanotech Ltd, Cambridge, UK) with 0.1 mm wide analytical gaps and a second stage differential mobility spectrometer with 0.5 mm analytical gap. The DMS analyser included Faraday plate detectors for positive and negative polarities to determine ion separations in the ultraFAIMS stage, the DMS stage, or the tandem ultraFAIMS/DMS instrument.

The ion source was a 2 mCi foil of ^{63}Ni located inside a 1/8″ stainless steel union (Swagelok Corp., Solon, OH, USA). Electronics and software for the ultraFAIMS stage were obtained from Owlstone Nanotech Ltd. Electronics and software for the DMS analyser were developed at New Mexico State University. Separate software was used to control ultraFAIMS and DMS stages from a single computer.

The carrier gas for tandem DMS was laboratory air at 1.5 L min^{-1} which was purified through 13X molecular sieve to a moisture level of 5 ppm$_v$, as measured by using Moisture Image Series 2 (Panametrics, Inc., Waltham, MA, USA). A model 5890 Series II gas chromatograph (Hewlett-Packard Corp., Avondale, PA) was used as an inlet for the tandem mobility analyser. The

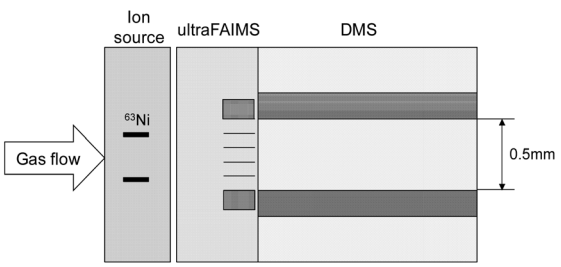

Fig. 1 Schematic representation of the ultraFAIMS/DMS analyzer.

chromatograph was equipped with a split–splitless injector and an SGE HT-5 (1.0 m long, 0.32 mm diameter, and 0.1 μm phase thickness) aluminium clad fused silica capillary column at 130 °C (Supelco Inc., Bellefonte, PA). The column was interfaced to the ultraFAIMS/DMS instrument through a 40 cm long and 1.5 mm OD stainless tube at 130 °C. Ambient pressure during the course of all experiments was 660 Torr.

Reagents and samples

Acetone, ethyl acetate, propyl acetate, and dimethyl methylphosphonate (DMMP) were obtained from Sigma-Aldrich, Inc. (St Louis, MO, USA) of the highest purity available. In studies with acetone, ethyl acetate and propyl acetate, a neat compound was drawn into a 10 μl syringe (Hamilton Company, Reno, NV) and slowly evaporated in the injection port at 60 °C. Vapour concentrations of 100–500 ppb were delivered to the ultraFAIMS/DMS analyser through the control of injector split ratios and total flows. In studies with DMMP, 0.3 ml of liquid in a 2 ml vial with a Teflon septum was fitted with a 0.6 mm ID by 25 mm long needle and placed in a glass bottle (Kintek, Houston, TX) for vapour generators. Air passed through this bottle provided 100–500 ppb with 10% or better absolute concentrations determined using gas chromatography/mass spectrometry. These different approaches to vapour delivery to ultraFAIMS/DMS resulted in different temperatures of the carrier gas, 40 °C for acetone, ethyl acetate and propyl acetate and 25 °C for DMMP.

Procedures

Individual spectra from the ultraFAIMS stage alone. Mobility spectra for an analyte were obtained from the ultraFAIMS stage with a fixed separation field (SF) and the DMS stage in all-pass mode. With a separation field (SF) of DMS of 0 Td, the compensation field (CF) was scanned from −0.1 to 0.1 Td repeatedly over 3 s with ~50 scans averaged. The scan of CF in the ultraFAIMS stage was from −2 to 2 Td in 300 s with 100 data points per spectrum. The signal was obtained from the detectors of the DMS stage.

Dispersion plots from the ultraFAIMS alone. Dispersion plots from the ultraFAIMS stage were constructed by combining CF scans obtained at SF values from 50 Td to 240 Td with the DMS stage in all-pass mode. A dispersion plot was generated in steps of 10 Td for the SF.

Full tandem operation of the ultraFAIMS/DMS analyser. Ions from a substance were characterized in full tandem ultraFAIMS/DMS mode where CF scan rates were 300 and 3 seconds per scan for the ultraFAIMS and DMS stages, respectively. A contour plot was generated using a matrix for all data points from all spectra.

Results and discussion

Performance test of tandem ultraFAIMS/DMS system

Results from the characterization of DMMP in a tandem ultraFAIMS/DMS measurement are shown in Fig. 2 as a contour plot of the ion intensity, compensation field in the ultraFAIMS stage at SF 100 Td and compensation field in the DMS stage at SF 50 Td.

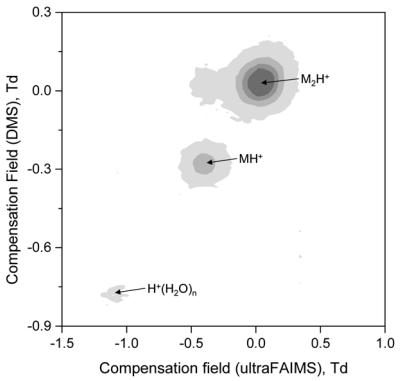

Fig. 2 Contour plots of ion intensity, compensation field in ultraFAIMS and compensation field in DMS for DMMP at 25 °C with the separation field in ultraFAIMS of 100 Td and the separation field in DMS of 50 Td.

Three ion peaks were baseline resolved and arise[23] in mobility spectra from $H^+(H_2O)_n$, $MH^+(H_2O)_m$ and $M_2H^+(H_2O)_p$, which are commonly termed the reactant ion, the protonated monomer, and the proton bound dimer and simplified here as $H^+(H_2O)_n$, MH^+ and M_2H^+. Peak positions are pairs of CF values for ultraFAIMS and DMS stages as −1.1, −0.78 for $H^+(H_2O)_n$; −0.37, −0.28 for MH^+; and 0.06 and 0.04 Td for M_2H^+. A peak of minor intensity at −0.37, 0.04 is understood as an ion passing the ultraFAIMS stage as the MH^+ with a CF of −0.37 Td and undergoing between the ultraFAIMS and DMS stages a clusterization reaction with residual M to form M_2H^+ which passes the DMS stage at 0.04 Td.

Peak widths can be defined in both dimensions of CF for the ultraFAIMS and DMS stages and were (Td): 0.13, 0.06 for the reactant ion; 0.39, 0.19 for MH^+, and 0.52, 0.3 for M_2H^+. The narrow peak widths with the DMS stage arise from comparatively long residence times of ions in a stage, 2 ms for the DMS stage compared to ~100 μs for the ultraFAIMS stage. This is thought to arise from an effective narrowing of the inlet aperture through losses of ions at the edges of ion swarms with prolonged cycles of oscillation in the analyser. In other aspects of analytical performance in Fig. 2, ions derived from DMMP were not completely resolved in the ultraFAIMS at 100 Td and baseline separation of ion peaks was achieved only in the tandem measurement with additional separation power provided by the DMS stage where an SF of 50 Td in the 13 mm long DMS stage provided improved peak capacity over the ~1 mm long ultraFAIMS stage with an SF of 100 Td. In addition to differences in ion residence time, these stages have characteristic waveforms, unaltered here, for the separation field and these are known to affect resolving power. Finally, peak intensities in Fig. 2 reflect vapour concentrations of DMMP and the residual reactant ion suggests that the source is not saturated at the calibrated vapour concentration of 100 ppb.

The results in Fig. 2 demonstrate that an ultraFAIMS stage could be directly coupled to the DMS stage providing tandem mobility measurements consistent with prior DMS/DMS findings and that performance of the ultraFAIMS/DMS instrument was adequate though electronics were not integrated or synchronous and were controlled manually. The reaction of residual M with MH^+ in the interface between two stages suggests that flow patterns and residence times were not optimized, though the intensity of this artefact peak is relatively low.

Dissociation of small proton-bound dimer ions in ultraFAIMS with DMS in all pass modes

The influence of electric fields on ion behaviour can be explored with field asymmetric waveform mobility methods conveniently as seen in Fig. 3a for ethyl acetate where the SF of ultraFAIMS was swept from 50 to 125 Td.

In this dispersion plot, the field dependence of mobility for the reactant ion, MH^+ and M_2H^+ shows characteristic patterns where the reactant ion peak exhibits a positive alpha function until −0.45 Td at an SF of 65 Td after which losses in ion transmission exhaust the ion current at the detector. Dependences for the MH^+ and M_2H^+ show positive and negative alpha functions, respectively, consistent with relatively small ions. The traces for the MH^+ peak extend to an SF of 110 Td and that for the M_2H^+ peak to 103 Td. In Fig. 3b, derived from Fig. 3a, peak intensities for MH^+ and M_2H^+ ions as a function of separation field in ultraFAIMS are shown. Here the intensity of the monomer, which is a predominant peak at 80 Td SF, decreases faster than that of the dimer peak with the increase in separation field strength. Quantitative details are further seen in individual ultraFAIMS spectra at SF values of 90, 100 and 110 Td (Fig. 4a) where peak heights are 0.7, 0.5 and 0.2 V for the M_2H^+ and ~0.5, 0.5 and 0.38 V for the MH^+. Ratios for peak heights of MH^+ to M_2H^+ are plotted against SF (Fig. 4b) and can be compared to a similar plot for DMMP.

The ratio of peak intensities for DMMP is 0.75 below 90 Td and 0.65 above 100 Td, constituting a control measurement where MH^+ and M_2H^+ pass through the ultraFAIMS without transformations. A slight decrease in ratios occurs through a mass dependent transmission bias against small mass ions. In contrast, the increase in ratio for ethyl acetate can be attributed to dissociation of the M_2H^+ to MH^+ through increases in ions' effective temperature (T_{eff}) from electric field heating. A line extrapolated between 120 and 100 Td to a baseline suggests the onset of dissociation at ~96 Td and 40 °C. The significance of this finding is that ions which form peaks that cluster near 0 Td in CF, limiting the analytical space under a purified gas atmosphere, can be transformed using electric field heating to form ions with peaks with other CF values. While this is possible with a single stage only, a comprehensive measure of ion behaviour is possible in a tandem measurement.

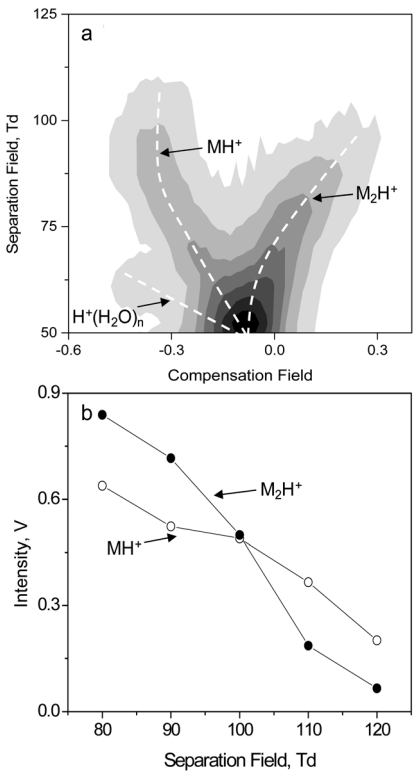

Fig. 3 Dispersion plot of ethyl acetate (a) and the intensity of its monomer and dimer ions (b) at 40 °C in ultraFAIMS.

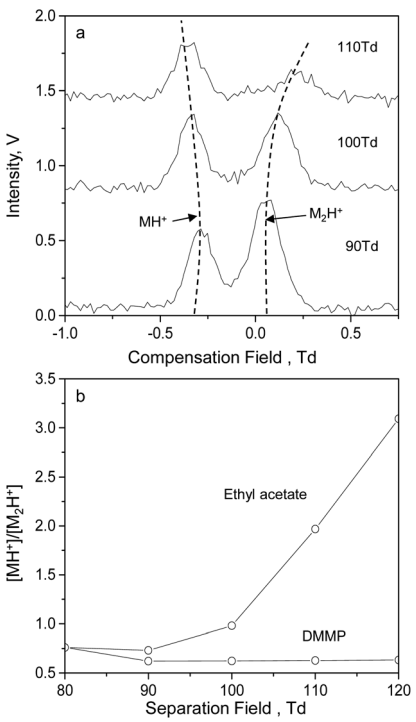

Fig. 4 Differential mobility spectra of ethyl acetate at 40 °C for various separation fields in ultraFAIMS (a) and the change in the monomer to dimer ion ratio for ethyl acetate and DMMP as a function of separation field strength (b).

Dissociation of small proton-bound dimer ions in tandem ultraFAIMS/DMS

The selectivity with ion dissociation in a comprehensive tandem ultraFAIMS/DMS measurement is shown in contour plots (Fig. 5a) with the ultraFAIMS stage at SF 87 Td and the DMS stage at 40 Td. When the SF for the ultraFAIMS stage is increased to 100 Td (Fig. 5b), the M_2H^+ peak is eliminated, while the MH^+ peak and the artefact peak (similar to that shown in Fig. 2) persist.

The benefit of a tandem mobility measurement can be seen directly as a simplification of response. Since M_2H^+ peaks tend to cluster near 0 Td while protonated monomers are distributed over an increased span of CF values, the conversion of M_2H^+ peaks to ions with larger CF values should provide an improved peak capacity without a gas modifier to alter alpha functions. This is demonstrated here only indirectly by elimination of the dimer peak appearing at a compensation field in DMS dimension at 0.02 Td and preserving the monomer peak appearing at −0.2 Td. Nevertheless, the importance of these findings is that ions can be dissociated in a first stage of a tandem mobility system and the products of dissociation can be characterized in a second mobility stage, all in air at ambient pressure. In addition, there was little effort to optimize the geometry and waveforms of each stage, and ion losses should be significantly improved with symmetric waveforms with comparable frequencies and field strengths to those used in the asymmetric waveform of the ultraFAIMS.

Shifting the peak position on the CF scale when ions are dissociated in a tandem mobility analyzer is one way of enhancing selectivity through ultraFAIMS/DMS measurements. Another parameter which can potentially be used to discriminate against some components in a mixture analysis is the onset field for ion dissociation. To examine the effect of ion mass on the value of onset field for dissociation, acetone, a molecule which forms a dimer ion with a structure similar to that of the ethyl acetate dimer ion but with smaller mass, was chosen. Dissociation of the M_2H^+ for acetone is shown in contour plots of Fig. 6, paralleling those of ethyl acetate although SF values in the ultraFAIMS differ significantly from those for ethyl acetate.

Ion peaks for the MH^+ and M_2H^+ (SF of 70 Td for ultraFAIMS stage and 40 Td for DMS stage) showed CF pairs of −0.36, −0.33 Td and 0.0, −0.05 Td, respectively. When the ultraFAIMS stage was set to an SF of only 87 Td, the M_2H^+ ion was dissociated to MH^+ (Fig. 6b). The plot was simplified with a loss of peak intensity for M_2H^+ from dissociation to MH^+. The difference in field strength to dissociate M_2H^+ peaks of ethyl acetate (100 Td) and acetone (87 Td) is understood to arise from differences in the number of vibrational degrees of freedom of ions among which the energy gained by the ion from the electric field should be distributed before the dissociation is possible. This value is determined by the number of atoms in the ion ($3N - 6$) and is higher for M_2H^+ of ethyl acetate than that of acetone. The SF for onset of dissociation at a given temperature is proportional broadly to ion mass and

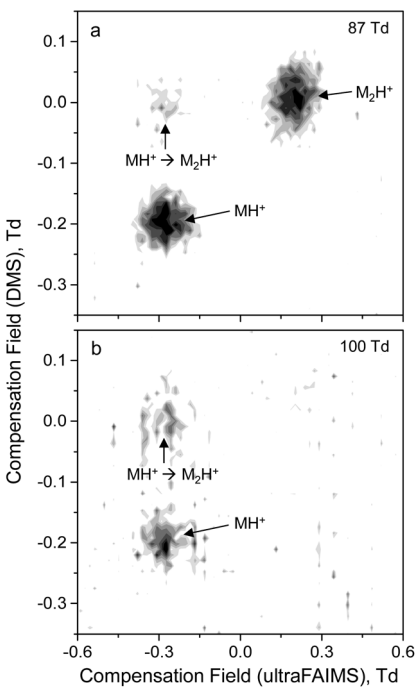

Fig. 5 Contour plots of ion intensity, compensation field in ultraFAIMS and compensation field in DMS for ethyl acetate at 40 °C with separation fields in ultraFAIMS of 87 Td (a) and 100 Td (b) and the separation field in DMS of 40 Td for both plots.

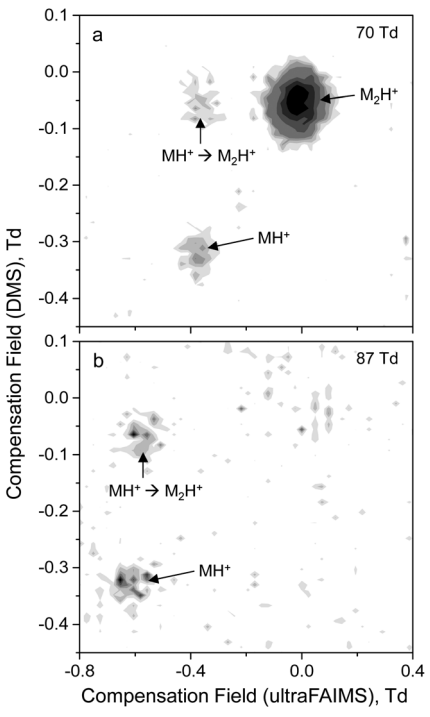

Fig. 6 Contour plots of ion intensity, compensation field in ultraFAIMS and compensation field in DMS for acetone at 40 °C with separation fields in ultraFAIMS of 70 Td (a) and 87 Td (b) and the separation field in DMS of 40 Td for both plots.

can provide an additional dimension of selectivity in the determination of ions.

Dissociation of higher mass ions in ultraFAIMS/DMS

Dissociation of M_2H^+ for DMMP, with a mass ~1.5× greater than M_2H^+ for ethyl acetate, was possible at room temperature with the strong fields available in the ultraFAIMS stage as shown in Fig. 7.

The dashed line in the dispersion plot shows the upper limit for SF with the in-house built DMS technology. Persistence of the MH^+ peak on a separation field scale of Fig. 7 until 220 to 230 Td and its nearly equal intensity to that of the dimer peak at these separation fields suggests the dissociation of M_2H^+ of DMMP to MH^+. This observation was further explored with individual high field mobility spectra derived from dispersion plots.

Mobility spectra at three SF for the ultraFAIMS stage are shown in Fig. 8a for MH^+ and M_2H^+ where changes in the SF cause changes in CF values (dashed lines) and also changes in the ion peak intensities. These were 1.2, 1.2, and 1 V for MH^+ and 3.5, 2.3, and 1 V for M_2H^+ at separation fields of 100, 180 and 200 Td, respectively. The ratio of peak intensities for MH^+ to M_2H^+ is plotted in Fig. 8b, changing from 0.34 to 1 between SF of 100 Td and 200 Td.

The ratio slightly decreases from 0.35 at 100 Td to 0.28 at a separation field of 140 Td and increases rapidly from 150 Td, reaching a value of 1.0 at the separation field of 200 Td. Extrapolation of the curve from 170 to 200 Td onto a baseline yields an onset SF of 160 to 170 Td. Comparison of the ratios at 200 Td and 160 to 170 Td shows a 2 to 3 fold increase, which is smaller than that for ethyl acetate, which was capped at 150 Td. Data in Fig. 8 show the dissociation at room temperature of a proton bound dimer ion with mass 1.5 and 2 times greater than that of ethyl acetate and acetone, respectively.

Contour plots from a tandem ultraFAIMS/DMS analysis of DMMP are shown in Fig. 9 with three peaks, MH^+, M_2H^+ and the artefact peak, at an SF of 150 Td in the ultraFAIMS stage and 50 Td in the DMS stage. When a field is increased from 150 Td to 200 Td in Fig. 9b, an artefact peak is undetectable,

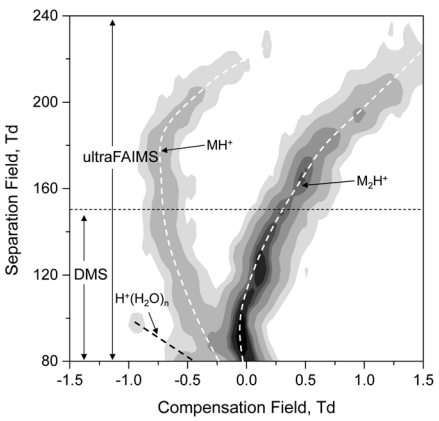

Fig. 7 Dispersion plot of DMMP at 25 °C in ultraFAIMS.

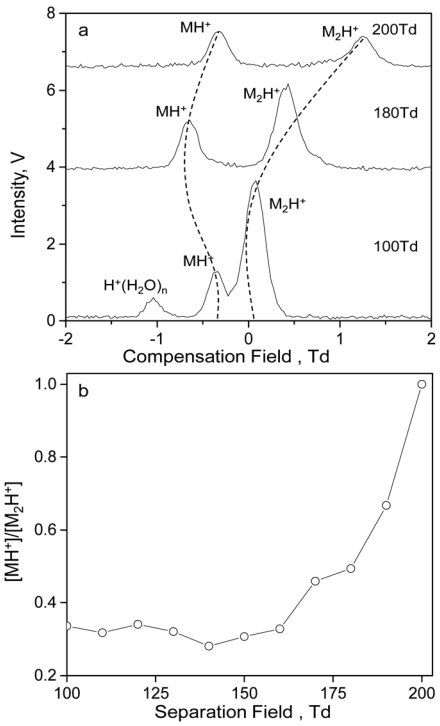

Fig. 8 Differential mobility spectra of DMMP at 25 °C for various separation fields in ultraFAIMS (a) and the change in the monomer to dimer ion ratio as a function of the separation field strength (b).

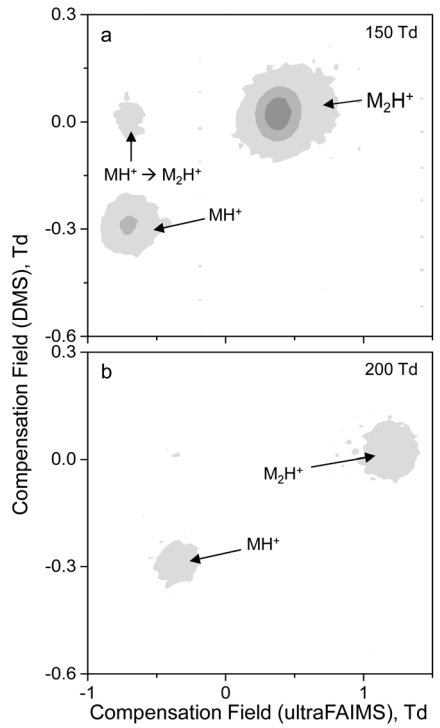

Fig. 9 Contour plots of ion intensity, compensation field in ultraFAIMS and compensation field in DMS for DMMP at 25 °C with separation fields in ultraFAIMS of 150 Td (a) and 200 Td (b) and the separation field in DMS of 50 Td for both plots.

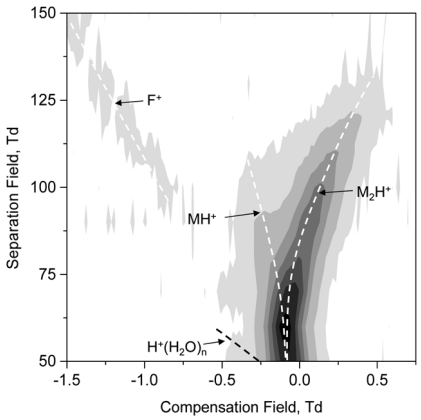

Fig. 10 Dispersion plot of propyl acetate at 40 °C in ultraFAIMS.

while MH^+ and M_2H^+ peaks' intensities drop from 0.8 to 0.55 and from 1.8 to 0.6 V, respectively. The peak ratio changes from 0.44 to 0.92, an increase of 2 times, consistent with the results in Fig. 8. The dimer of DMMP in Fig. 9b is not eliminated completely at a separation field of 200 Td and even higher electric fields may be valuable providing losses in ion transmission can be mitigated. These findings are the first description where the first stage of a tandem mobility instrument was used to dissociate an ion of such a size and a second stage was used for mobility separation.

Ion fragmentation with electric fields in ultraFAIMS with DMS in all pass modes

A dispersion plot for propyl acetate in the ultraFAIMS/DMS instrument at a slightly elevated temperature, 40 °C, is shown in Fig. 10 and includes patterns for MH^+, M_2H^+ and reactant ion peaks.

Significantly, the ion peak for MH^+ of propyl acetate is lost at a low SF value and a new ion peak appears faintly at an SF of ~90 Td. Such a behaviour for propyl acetate was previously documented in DMS[29] and a newly appearing peak was determined to be the protonated molecule of acetic acid formed by the fragmentation of MH^+ of propyl acetate. Another product of this reaction was propene.

These findings suggest that tandem measurements with the ultraFAIMS/DMS instrument may include a combination of thermal and electric heating for ion fragmentation in the ultraFAIMS stage with subsequent characterization of product ions in a second, DMS, stage. Fragment ions commonly have large positive alpha functions and appear at even more negative compensation fields than monomers (Fig. 10). In addition, fragment ions may be suggestive of chemical families of compounds from which they were formed.[32]

Conclusions

Tandem mobility concepts with DMS will advance when ions can be transformed between DMS stages to introduce chemical orthogonality with user control of chemical processes. The dissociation or fragmentation of ions through increases in ion effective temperature by electric field heating constitutes a fast and relatively cool method to alter ions. In this work, the basis for such transformations has been established using commercially available technology, the ultraFAIMS stage (250 Td maximum), in combination with a DMS stage which exhibits an improved peak capacity through comparatively low field strengths (150 Td maximum). The goal of ion dissociation in one mobility stage and ion characterization in a second stage was achieved although poor transmission efficiency above 100 Td in the ultraFAIMS stage lessened the overall ion intensity. This suggests the need for optimization of structures or electronics for ion heating.

Acknowledgements

The financial support from the National Science Foundation, award No. 1306388, and ChemRing Detection Systems is gratefully acknowledged. Machine shop contributions from John Tobin and help with an UltraFAIMSK-DK1 Developer Kit from Danielle Toutoungi of Owlstone Ltd (Cambridge, UK) were received gladly in this project. Authors are especially grateful to Dr John Stone, professor emeritus of Queens University of Canada, for continuous support of the project.

Notes and references

1 I. A. Buryakov, E. V. Krylov, E. G. Nazarov and U. K. Rasulev, *Int. J. Mass Spectrom. Ion Processes*, 1993, **128**, 143–148.
2 R. A. Miller, G. A. Eiceman, E. G. Nazarov and A. T. King, *Sens. Actuators, B*, 2000, **67**(3), 300–306.
3 A. A. Shvartsburg, K. Tang and R. D. Smith, *J. Am. Soc. Mass Spectrom.*, 2004, **15**(10), 1487–1498.
4 J. G. Bryant, M. Prieto, T. A. Prox and R. A. Yost, *Int. J. Mass Spectrom.*, 2010, **298**(1–3), 41–44.
5 R. W. Purves, R. Guevremont, S. P. Day, W. Charles and M. S. Matyjaszczyk, *Rev. Sci. Instrum.*, 1998, **69**, 4094–4104.
6 R. W. Purves and R. Guevremont, *Anal. Chem.*, 1999, **71**, 2346–2357.
7 B. B. Schneider, T. R. Covey, S. L. Coy, E. V. Krylov and E. G. Nazarov, *Int. J. Mass Spectrom.*, 2010, **298**(1–3), 45–54.
8 A. A. Shvartsburg, R. D. Smith, A. Wilks, A. Koehl, D. Ruiz-Alonso and B. Boyle, *Anal. Chem.*, 2009, **81**, 6489–6495.
9 G. A. Eiceman, Z. Karpas and H. H. Hill, *Ion Mobility Spectrometry*, Taylor &Francis/CRC Press, Boca Raton, FL, 3d edn, 2014, pp. 35–36, 296–297.
10 T. F. Limero, P. Cheng and J. J. Boyd, *Int. J. Ion Mobility Spectrom.*, 2006, **9**(1), 29–34.
11 E. V. Krylov and E. G. Nazarov, *Int. J. Mass Spectrom.*, 2009, **285**(3), 149–156.

12 Z. Karpas and Z. Berant, *J. Phys. Chem. A*, 1989, **93**(8), 3021–3025.
13 Z. Karpas, G. A. Eiceman, E. V. Krylov and N. Krylova, *Int. J. Ion Mobility Spectrom.*, 2004, **7**(1), C8–C18.
14 N. Krylova, E. Krylov and G. A. Eiceman, *J. Phys. Chem. A*, 2003, **107**(19), 3648–3654.
15 L. C. Rorrer III and R. A. Yost, *Int. J. Mass Spectrom.*, 2010, **300**(2–3), 173–181.
16 G. A. Eiceman, E. V. Krylov, N. S. Krylova, E. G. Nazarov and R. A. Miller, *Anal. Chem.*, 2004, **76**(17), 4937–4944.
17 D. S. Levin, R. A. Miller, E. G. Nazarov and P. Vouros, *Anal. Chem.*, 2006, **78**(15), 5443–5452.
18 B. B. Schneider, E. G. Nazarov and T. R. Covey, *Int. J. Ion Mobility Spectrom.*, 2012, **15**(3), 141–150.
19 B. B. Schneider, T. R. Covey and E. G. Nazarov, *Int. J. Ion Mobility Spectrom.*, 2013, **16**(3), 207–216.
20 D. S. Levin, R. A. Miller, E. G. Nazarov and P. Vouros, *Anal. Chem.*, 2006, **78**(15), 5443–5452.
21 V. Blagojevic, A. Chramow, B. B. Schneider, T. R. Covey and D. K. Bohme, *Anal. Chem.*, 2011, **83**(9), 3470–3476.
22 V. Blagojevic, G. K. Koyanagi and D. K. Bohme, *J. Am. Soc. Mass Spectrom.*, 2014, **25**(3), 490–497.
23 E. G. Nazarov, S. L. Coy, E. V. Krylov, R. A. Miller and G. A. Eiceman, *Anal. Chem.*, 2006, **78**, 7697–7706.
24 M. R. Menlyadiev and G. A. Eiceman, *Anal. Chem.*, 2014, **86**(5), 2395–2402.
25 G. A. Eiceman, D. B. Shoff, C. S. Harden and A. P. Snyder, *Int. J. Mass Spectrom. Ion Processes*, 1988, **85**(3), 265–275.
26 R. G. Ewing, G. A. Eiceman, C. S. Harden and J. A. Stone, *Int. J. Mass Spectrom.*, 2006, **255–256**, 76–85.
27 M. Y. Rajapakse, J. A. Stone and G. A. Eiceman, *J. Phys. Chem. A*, 2014, **118**(15), 2683–2692.
28 X. An, G. A. Eiceman and J. A. Stone, *Int. J. Ion Mobility Spectrom.*, 2010, **13**(1), 26–36.
29 X. An, G. A. Eiceman, J. E. Rodriguez and J. A. Stone, *Int. J. Mass Spectrom.*, 2011, **303**(2–3), 181–190.
30 E. G. Nazarov, S. L. Coy, E. V. Krylov, R. A. Miller and G. A. Eiceman, *Anal. Chem.*, 2006, **78**(22), 7697–7706.
31 L. J. Brown, R. W. Smith, D. E. Toutoungi, J. C. Reynolds, A. W. Bristow, A. Ray, A. Sage, I. D. Wilson, D. J. Weston, B. Boyle and C. S. Creaser, *Anal. Chem.*, 2012, **84**(9), 4095–4103.
32 S. E. Bell, E. G. Nazarov, Y. F. Wang, J. E. Rodriguez and G. A. Eiceman, *Anal. Chem.*, 2000, **72**, 1192–1198.

